Performance of dissimilar metal Self-Piercing Riveting (SPR) joint and coating behaviour under corrosive environment

H. R. Kotadia[1], A. Rahnama[1], I.R. Sohn[2], J. Kim[2], S. Sridhar[1,3]

[1] Warwick Manufacturing Group, The University of Warwick, Coventry CV4 7AL, UK

[2] POSCO Research Labs, 8, Pokposarang-gil, Gwangyang-si, Jeonnam 545-875, South Korea

[3] George S. Ansell Department of Metallurgical and Materials Engineering, Colorado School of Mines, Golden, CO 80401, USA

Abstract:

The present paper investigates the effect of corrosive environments on the degradation and mechanical properties of Self-Piercing Riveting (SPR) joints between dissimilar metals. The investigations were carried out on a lap-shear joint of 5182 aluminium with pure zinc (GI), and a zinc—aluminium—magnesium (ZM or PosMAC® 1.5) coated 590DP steel. The experimental results show that corrosion significantly influences the lap shear performance and failure mechanism of the joint depends on the type of coating and pre-treatment with and without primed (80% zinc, 10% aluminium). Detailed microstructural analysis of the SPR specimen and coating reveal the actual mechanism for mechanical property degradation. In ZM coated steel the formation of Mg^{2+} and Al^{3+} ions delay transformation of basic zinc salts to ZnO, and thereby retard the rate of corrosion. The experimental evidence supports the proposition that ZM coated steels have four-times superior corrosion resistance compared to zinc-coated steels.

Keywords: Dissimilar material joining; Self-Pierce Rivet; Corrosion; 590DP steel; Aluminium.

1. Introduction

The lightweighting vehicles have received significant attention in recent years, in order for automotive manufacturers to achieve better fuel efficiency to meet greenhouse emission targets [1, 2]. Simultaneously, automotive manufacturer have to satisfy safety requirements i.e. collision safety, pedestrian protection and other customer demands [3]. Various measures have been taken to reduced fuel consumption including new powertrains involving hybrid systems or advanced diesel engines, reduced vehicle size, optimised design, and replacement of materials used in its construction with lighter mass alternatives [3]. The strategy materials substation with lighter alternative has been pursued to great extent, and now aluminium is widely used in the automotive industry. The advantage of aluminium over other lightweight metals lies in its strength-to-ductility ratio, toughness and its inherent corrosion resistance with no need for an additional coating [4]. Nevertheless, it is unlikely that automobiles can ever be manufactured using only aluminium for applications such as crash protection, battery casings etc. [5]. It therefore becomes important to develop strategies and techniques, which can join dissimilar metals such as aluminium to steel [6]. There are many joining techniques available and these can be classified in three, categories:

i. Fusion welding including Resistance Spot Welding (RSW) [7], laser welding [8, 9], arc welding [10] etc.,
ii. Solid state joining including friction welding [11], and
iii. Mechanical joining including Self-Pierce Riveting (SPR) [12], laser and friction riveting [13] etc.

All the fusion techniques mentioned have been successfully used in automotive manufacturing industries, however, they have been less successful joining dual phase (DP) steels, coated steels and dissimilar metals because of the tendency to soften in the Heat Affected Zone (HAZ) in DP steels, Liquid Metal Embrittlement (LME) is observed Zn coated steels, severe segregation, the formation of hard intermetallics and hot cracking are commonly observed, when dissimilar metal are welded [5, 6]. During conventional welding techniques, additional material is added through a filler wire to produce desirable weld joints. The deposited additional metal will however, increase weight, cost and the quality of the result can be limit for specific materials. Remote Laser Welding (RLW) has gained popularity because of its distinct advantages such as design flexibility, material (and cost) saving and improved productivity [14, 15]. Friction welding is also a attractive option to join dissimilar materials and has achieved success in aerospace industry [16, 17]; however, it does not provide design flexibility and is expensive for deployment in mass production applications.

Traditionally RSW is used for steel vehicles fabrication and a typical modern car body in white (BIW) contains 4,000-6,000 spot welds [7]. Changing materials in order to facilitate lightweight manufacturing presents many challenges in respect to implementing available RSW welding techniques economically for high volume production whilst maintaining acceptable weld quality. There are various challenges to weld Al through RSW such as: high thermal conductivity and strong stable oxide films on the surface. Both

these effects result in the requirement of a high energy input which in turn result in increased electrode wear and requirement for cleaning [18]. Compared with RSW, the SPR technology is a cold process therefore; there is detrimental effect in the substrate due to a HAZ. Additional advantages of SPR are, low energy requirement and high tool life [12]. However, SPR also has limitations such as the requirement of a access to both sides of the material, the cost and weight associated with the rivet, more complex recycling and possible galvanic corrosion issues etc [12].

In case of dissimilar metal joining, particular in the case of steel/aluminium, there is an increased risk of corrosion due to the difference in electrochemical behaviours of two the metals [19, 20]. This behaviour is identified as being galvanic corrosion. The mitigation of galvanic corrosion is critical especially in the location around the rivet joint. The variance in electrochemical behaviour, leads to degradation of the mechanical properties of the joint (i.e fatigue strength). This occurs mainly through a thinning process, which takes place in the less noble metals due to penetration of corrosion media through part gaps, such as the overlapping areas. In addition, the riveting operation generates significant residual stresses, which further accelerate the corrosion process. In order to address the concerns regarding corrosion issues and, the considerable cost associated with this problem; steel companies have developed advanced coatings. The popular coatings used by the steel industries are Zn, Zn-Mg and Zn-Al-Mg for steel targeted at the construction, home appliances and automotive industries [21].

It appears that despite the large volume of literature published on SPR processes and mechanical properties, there are only few studies [20, 22-24] on effect of corrosion environment and its influence on the degradation of mechanical properties and eventual failure mechanism. In present investigation explore the dissimilar joining of a commercially available 5182 aluminium alloy and 590DP (dual phase) steel sheet with either a Zn coated or Zn-Al-Mg coated steel. The performance of the joint is evaluated after salt spray. Finally, an attempt is made to elucidate the corrosion mechanisms for Zn and Zn-Al-Mg coated steel and fracture mechanisms once the joint is exposed to a corrosive environment.

2. Experimental procedure

2.1 Material and sample preparation

The material used in this study is commercially available 1.5 mm thick 5182 aluminium sheet with a standard pre-treatment H111 and wax lubricant (AL070) and a 590DP steel sheet with Zn coated and Zn-Al-Mg coated, called GI and ZM, respectively. Coating weight for GI and while PosMAC® are 60 g/ m^2 and 35 g/ m^2, respectively. The compositions of 5182 and 590DP steel are listed in Table 1. The 5182 has UTS of 260 MPa, yield strength h of 220 MPa and elongation of 22%. 590DP steel has UTS of 590 MPa, yield strength of 418.3 MPa and elongation of 25%.

Sheet metals were cleaned by acetone to remove protected lubricant and cut on rolling direction by using a guillotine press. Specimen geometries and dimensions for lap shear test is shown in Fig. 1. Three sets of

samples were prepared on two coated steel for the corrosion test: as received material, painted with primer (both side) before riveting, painted with primer after riveting (only visible area), here it's called A, B, C, respectively. Primer contain 80 wt.% Zn, 10 wt.% Al. All three prepared configurations are shown in Fig. 2. Tests and analyses on individual samples are summarised in Table 2. Experiments with the primer was conducted to provide additional understanding of the corrosion mechanism with additional protective layer on the base material.

All the configurations were produced by using Tucker riveting equipment. The steel rivets (countersunk head) coated with zinc/tin were also supplied by Tucker Ltd.. A specimen rivet/die/velocity combination was selected to achieve good joint quality (Table 3). During riveting the design fixture was used to reduce any variations in rivet position. After the completion of riveting, samples were cross-sectioned and analysed under the optical microscope in order to check SPR joint quality which includes interlock, head height and minimum remaining bottom sheet material thickness.

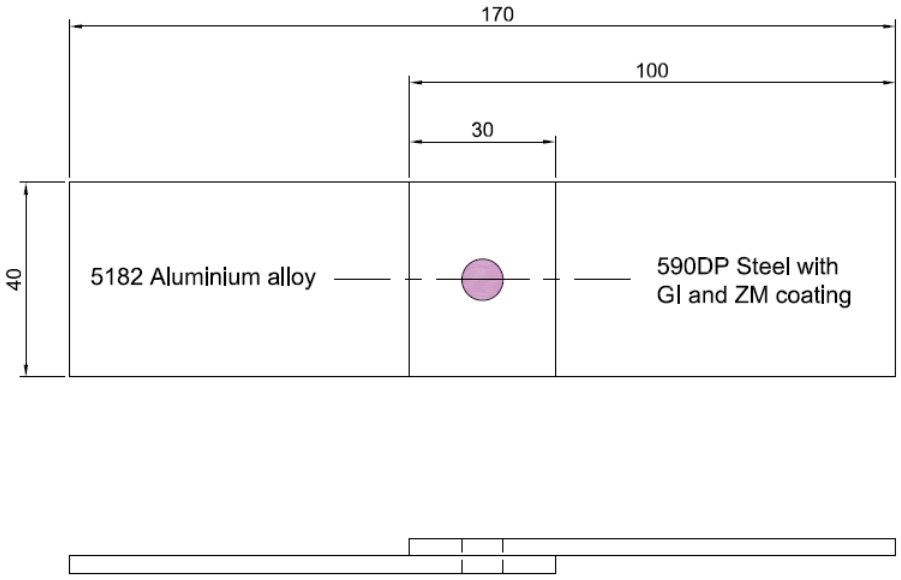

Fig. 1. Specimen geometry for lap-shear test.

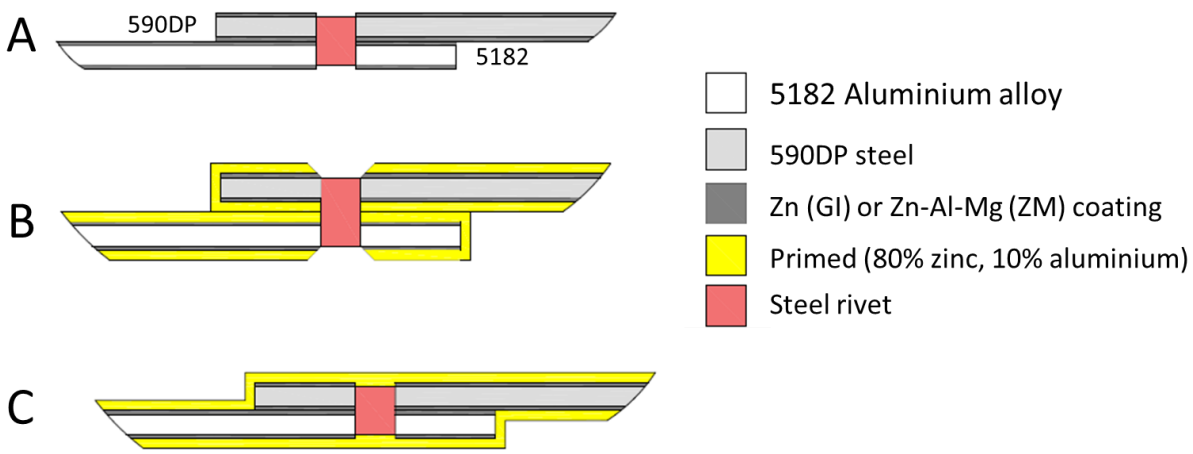

Fig. 2. Three sets of configurations (a) as received with coating - A, (b) painted with primer (both side) before riveting - B, and (c) painted with primer after riveting (only visible area) –C. Please note that in schematic illustration dimension are as per the real specimens i.e. thickness of coating and primer.

2.2 Corrosion test

An accelerated corrosion test was used to examine the rivet joint. The current study used up to 200 cycles, each cycle consists of a constant spray (ASTM B117 -16 [25]) of 5% NaCl solution at 35 °C for 2 h cycle and drying period of 2 h at room temperature. The specimens were removed from the salt chamber in regular intervals from 50 h to 200 h. After corrosion exposure, test samples were cleaned with ionised water before mechanical test and microstructure analysis.

2.3 Mechanical test

The lap shear specimens were mechanically tested before and after exposure to the accelerated corrosion test in order to evaluate the effect of corrosion on the mechanical properties of the joints, according to EN ISO 14273 [26]. Lap shear tensile tests were also conducted using an Instron 30 kN tensile testing machine. During the lap-shear test, spacers were used to grip the samples, in order to align the loading path and minimise the secondary bending.

2.4. Metallographic characterization

To understand supplied alloys and SPR the samples were crosssectioned and mounted in conductive compression phenolic resin (Bakelite). Samples for optical and Scanning Electron Microscope (SEM) examination were prepared to a 0.04 μm colloidal silica finish. The SEM was equipped with EDS and FIB to study elements and the cross section coating layer. The TEM samples were prepared by FEG and examination was performed at 200 kV on a JEOL JEM 2000FX-TEM equipped with a JEOL JED-2300T energy dispersive X-ray Spectrometer (EDS).

2.5 X-ray diffraction

The corrosion products on the corroded surface of the samples were characterized by X-ray diffraction (XRD) using a Panalytical Empyrean diffractometer equipped with Co(K_α) radiation and a solid state Pixel detector for fast data acquisition. For comparison, a supplied DP590 steel without being exposed to salt spray was also characterised. The analysed area was approximately 15 mm X 15 mm. The XRD was collected with a step size of ~0.013° over the angular range 5–90° (2θ) with a total collection time of 40 minutes. The evaluation of the data was done using the Panalytical HighScore Plus software package, containing the latest ICDD database files.

Table 1. 5182 Aluminium and 590DP steel alloy composition in wt.%.

Alloy	Al	Si	Fe	Cu	Mn	Mg	Cr	Zn
5182	Remaining	0.13	0.24	0.05	0.33	4.28	0.016	0.012
Alloy	Fe	C	Si	Mn	Cr	Mo		
590DP	Remaining	0.055	0.136	1.64	0.34	0.002		

Table 2. List of experiments and analysis on various samples.

Sample ID		Microstructure and SPR joint quality	Exposure to salt spray up to 200 h	Effect of salt spray on coating	Effect of salt spray on Lap-shear test
590DP (Zn coated)/5182	As received with coating - A	✓	✓	✓ (0 and 50 h)	✓ (0 to 200 h)
	Painted with primer (both side) before riveting - B	–	✓	–	✓ (0 to 200 h)
	painted with primer after riveting - C		✓	–	✓ (0 to 200 h)
590DP (Zn-Al-Mg)/5182	As received with coating - A	✓	✓	✓ (0 to 200 h)	✓ (0 to 200 h)
	Painted with primer (both side) before riveting - B	–	✓		✓ (0 to 200 h)
	painted with primer after riveting - C	–	✓	–	✓ (0 to 200 h)

Table 3: Rivet/die/velocity used for the experiments

Rivet	Length: 7.0 mm; Stem diameter: 5.35 mm; Type: countersunk; Hardness: ~410 Hv
Die	Cavity diameter: 11 mm; Cavity depth: 1.5 mm; Type: flat bottom
Velocity	100 mm/s (Tucker unit determining applied force)

3. Results

3.1. Microstructure analysis on sheet metals

The scanning electron micrograph from 5182 sheet is presented in Fig. 3a illustrating the ~ 3 μm size $Al_6(Fe, Mn)$ intermetallics particles (white in contrast) on an Al matrix. EBSD investigation (Fig. 3b) reveals equiaxed Al grain structure in the RD-ND plane of the sheet (RD: rolling direction, ND: normal direction), which can be attributed to the recrystallization kinetics associated with the rolling process. The average grain size, which was, measured 64 μm. The microstructure and EBSD image (RD-ND plane) of supplied 590DP steel sheet is presented in Fig. 3b and c. Dual phase steel consists of ferrite and minor

martensitic phases with the average of ~14 microns grain size. Supplied steel sheet coating characteristics are discussed in section 3.3.

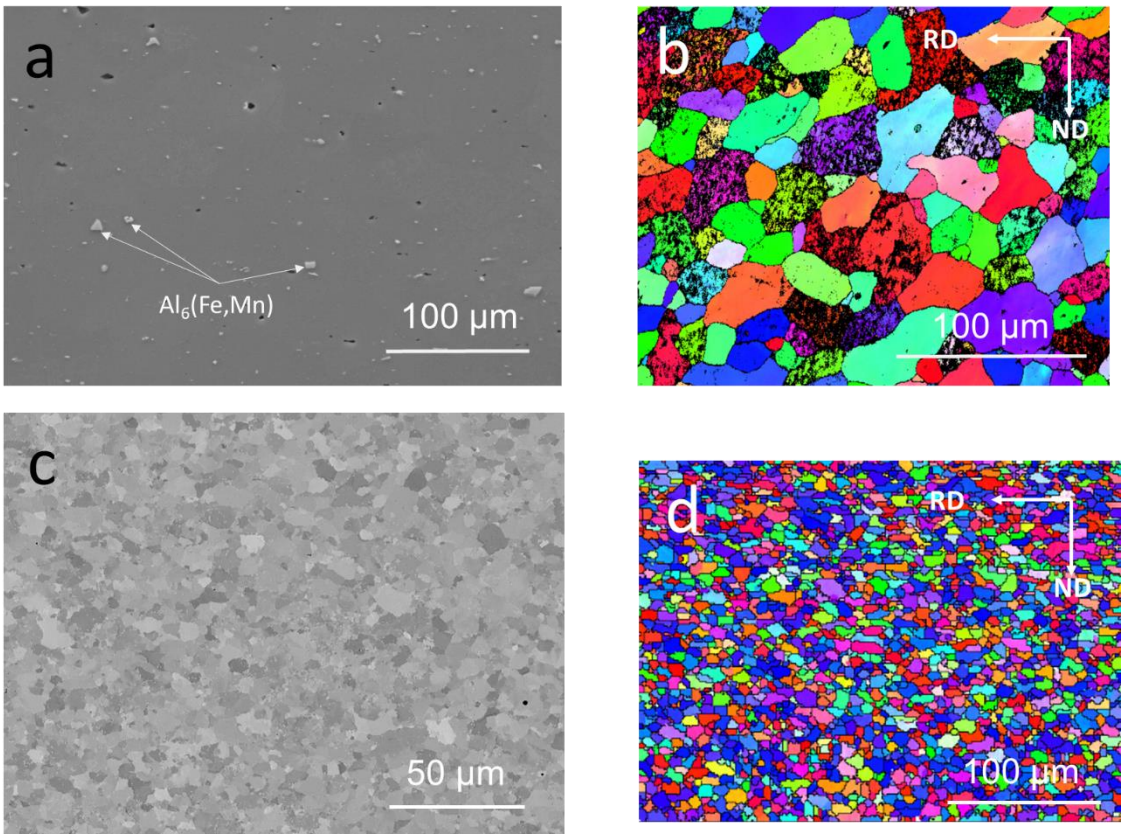

Fig. 3 Microstructure of received material (a), (b) 5182 alloy; (c), and (d) 590DP steel.

3.2 SPR joint quality

In order to produced strong and reliable joints, automotive industries have created joint quality criteria. Desirable joint quality can achieve by controlling SPR joint process and parameters [12]. Among these conditions, there are three main features that need to be measured and they are the rivet head height, the interlock distance and the minimum remaining bottom material thickness, as shown in Fig. 3. The SPR joint quality attributes have been annotated and an average interlock into Al of ≥ 1 mm, and a minimum remaining Al sheet (bottom) thickness of ≥ 0.3 mm. Under all three condition (A, B and C), joining observed very similar. It is worth noting that in SPR sheet metal, there was no pre-drilling or heating. Joining was achieved through rivet piercing the top sheet and interlocking at bottom sheet. Therefore, a difference of flow stress and ductility between the sheets is vital.

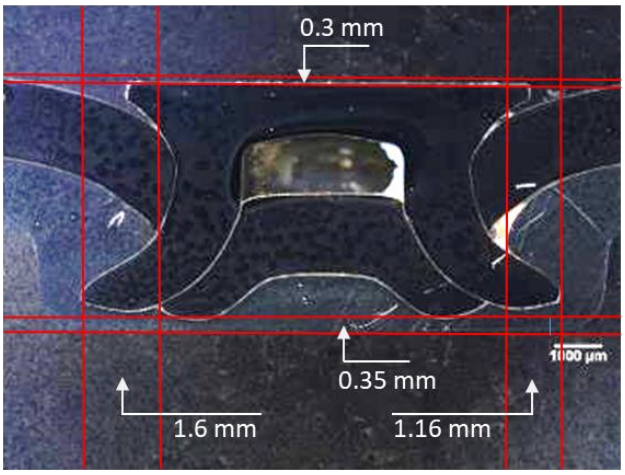

Fig. 4 Cross-section of SPR joints.

3.3. Effect of corrosion environment on coating

The microstructure of the top and the side view of Zn coated (GI) and Zn-Al-Mg coated (ZM) of the coated 590DP steel are shown in Fig. 5. Thickness's of GI and ZM coating measured 10 µm and 4 µm, respectively. The GI coated steel consists of a homogeneous pure Zn layer, while ZM coating consist of various phases, which are visible in Fig. 6. These phases identified as primary Zn grain with Al precipitation, binary Mg_2Zn –Zn and ternary eutectic Mg_2Zn-Zn-Al, and the interfacial intermetallics (IMCs) (with Al, Fe, Mn and Mg), which ensures a good adhesion of the coating on the steel surface [27].

The samples were exposed to salt spray for up to 200 h. The visual inspection and analysis showed different corrosion products or appearances. The GI sample shows zinc rust after 50 h of salt spray testing and its spread with time. After 200 h exposure, samples cover with thick corrosion product and significant amount of rust. By contrast, ZM coated steel shown minor suggestions of rust with thinner corrosion product even after 200 h exposure. Overall, visual examination shows substantial differences between both coatings. ZM has a significant enhance corrosion performance in salt spray test compared to GI.

Further examination on samples were carried out by making FIB cross-sections of the corroded specimens and investigating with SEM and EDS. Fig. 7 shows GI coated steel after 50 h exposure. At the top, there is a thick zinc – rich corrosion product 9 zinc – rich oxide) observed. In addition, cracks and pitting voids are visible on the coating, which can act as a channel to transport chlorine from the surface, creating a differential aeration cell and an autocatalytic situation, which accelerates corrosion between the substrate and coating. Subsequent exposure shows considerable corrosive attack of the steel substrate.

Fig. 8 shows a cross sectioned SEM micrograph of ZM coating after 50 to 200 h. A thin corrosion product is observed after exposure. EDS analysis shows high zinc and oxygen contents. Fig. 8a clearly reveals that corrosion initiation occurs from the eutectic areas and pure Zn grains are not affected. This suggest that eutectic $MgZn_2$ must be less noble compared to zinc grain and therefore corrodes preferentially. After 100 h, there is an increase in the thickness of the oxide layer and penetration. Fig. 8c shows a visible dark

corrosion product layer with significant amount of porosity in comparison with 50h. After 200 h exposure, the microstructure shows cracks, porosity and a gap between coating and substrate. However, the interfacial IMC and the substrate are not affected by corrosion.

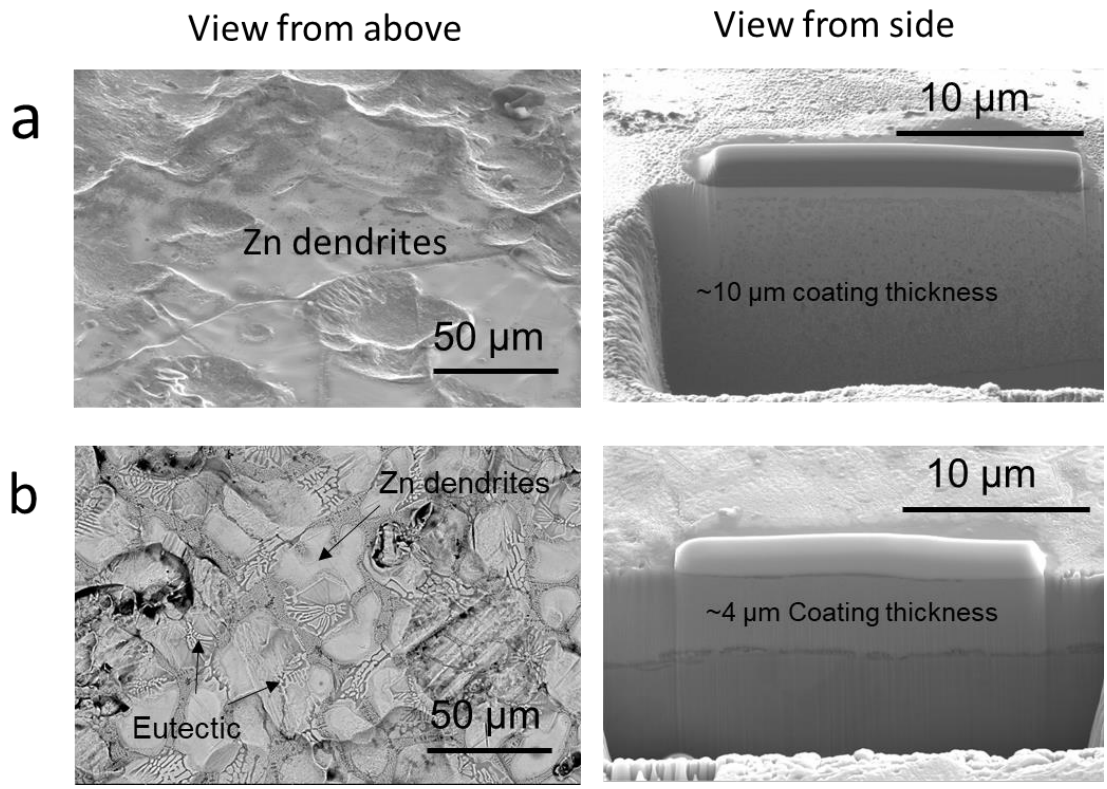

Fig. 5. SEM micrograph of (a) Zinc (GI) coating and (b) Zn-Al-Mg (ZM) coating view from above and side. Microstructures are showing various phases such as primary Zn dendrite and eutectic and coating thicknesses difference between GI and ZM coating..

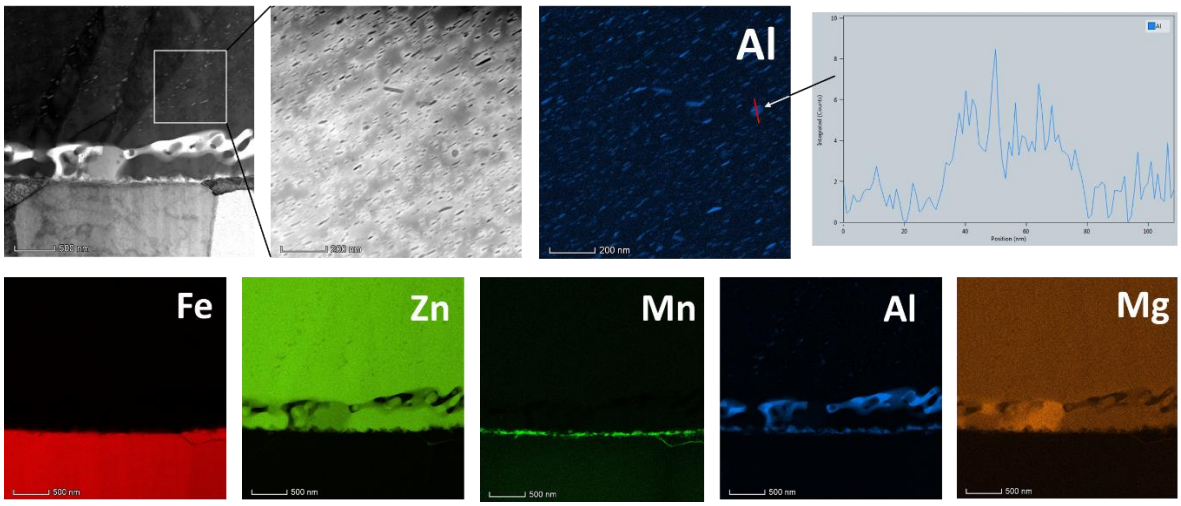

Fig. 6. TEM micrographs and EDs analysis of Zn-Al-Mg (ZM) coating, it's showing nano-precipitation of Al within the primary Zn grain and the composition of interfacial intermetallics.

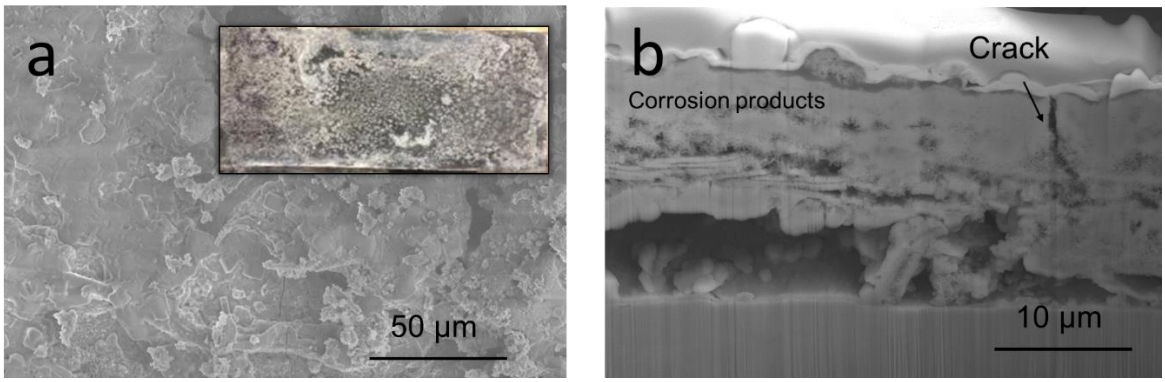

Fig. 7. SEM micrographs of Zn (GI) coating after 50 h exposure (a) showing the corrosion product (view from top) and (b) cross-section (view from side). Micrographs shown ZnO as corrosion product with crack and porosities within the coating.

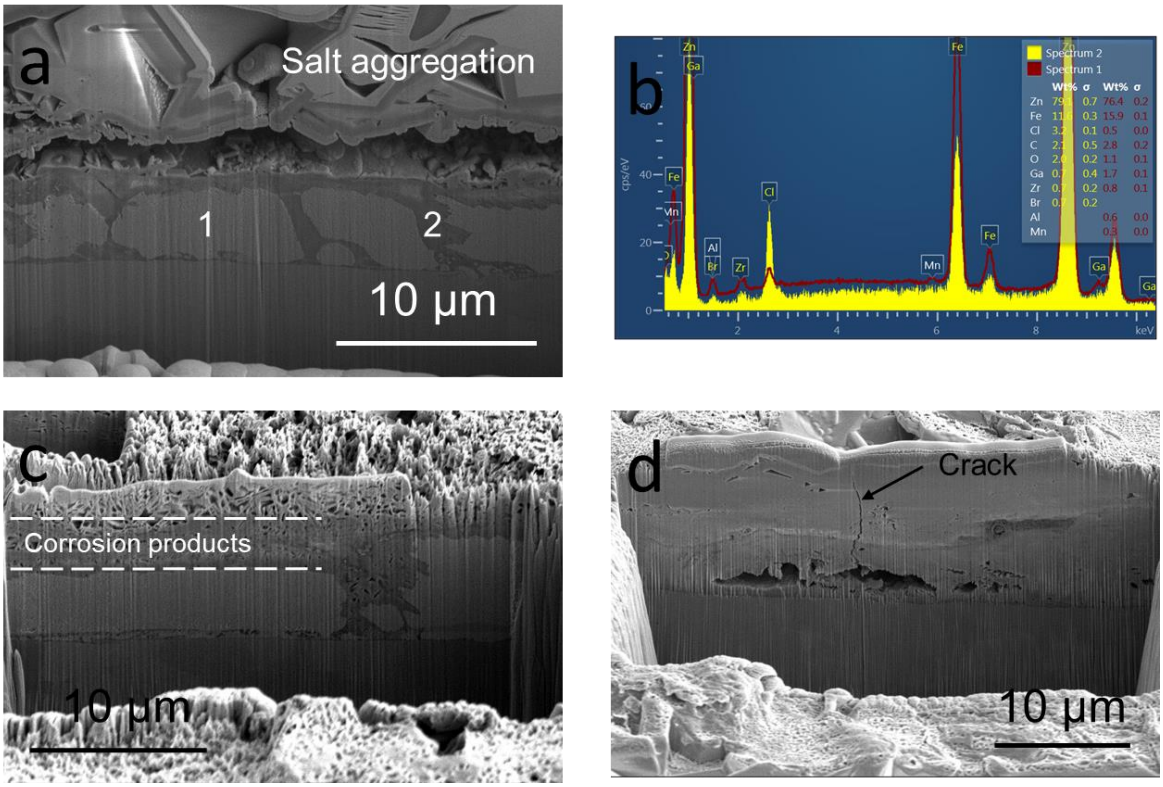

Fig. 8. SEM micrographs and EDS analysis of Zn-Al-Mg (ZM) coating after various time of exposure: (a) after 50 h (grey, in contrast, is Zn dendrites and dark grey, in contrast, is eutectic area), (b) EDS (spectrum 1 taken from Zn grain and spectrum 2 taken from the eutectic area of figure (a), showing higher chloride concentration), (c) after 150 h (progress in corrosion through eutectic dissolution and more porous structure in compare with figure (a), and (d) after 200 h (spalling and crack formation).

3.4 The effect of corrosion environments on mechanical properties and failure mechanisms

A single lap-shear sample prepared with various conditions (Table 2) was exposed to salt spray, and mechanical tests were carried out before and after exposure. In Fig. 9a, the load-displacement curve during the static lap shear test can be divided into three regions. Zone I is related to the deformation of the rivet and the sheet materials due to shearing load applied; Zone II shows the duration of the test staying around the maximum load level, and at the beginning of this region there is localised crack initiation on the aluminium side; Zone III shows the region that the joint starts the rapid failure. The Fig. 9b shows comparative load displacement curves of 5182/ GI coated steel and 5182/ZM coated steels. Testing results indicated that both coating have no influence on mechanical properties. Initially bearing stress concentrated at the point of contact of joint. As load increase cause yielding and the rivet on a larger area of contact and this results in more uniform stress [28], the nominal bearing resistance can be expressed as

$$\sigma_b = \frac{P}{t \cdot d} \quad (1)$$

where P denotes the load sustained by the rivet, t the sheet thickness and d the original rivet diameter. In the current experiment, top and bottom sheet thicknesses were the same, therefore, both sheets were subject to a similar tensile stress. However, tensile strength of the bottom aluminium sheet is lower than the top steel sheet consequently; it is likely failure would be expected to occur at the aluminium sheet before any deformation of the steel sheet. In addition, geometrical parameter, sheet thickness, riveting quality, exposure condition have significant influence on the failure mechanism.

In order to identify the evolution of the lap-shear test performance of the various configuration in function of the exposure time were plotted in Fig. 10 to 12. Three set of sample combinations (A, B, and C) were prepared and all the samples were subject to salt spray exposure and then a lap-shear test. The extended time in the salt spray environment leads to a different failure because in an aggressive environment condition the materials undergoes a noticeable degradation, as it is clearly noticed in a load–displacement curve and failed sample. The major difference observed was reduced displacement and good corrosion resistance achieved through the primer and ZM coating samples.

Case A (without primer): The GI coated steel joint shows significant reduction of displacement after 50 h of exposure and it was further reduced when the exposure time was increased further. In contrast to GI coated steel, the steel with ZM coating showed better resistance to corrosion exposure. It can be concluded that ZM coated joint are resistant to corrosion and take a longer time to corrode and subsequently weakening the joint. Various corrosion products from the overlapped lap-shear sheets area and its influence of interlocking the Al/steel sheets. Regarding Zone III, there is significantly reduced displacement due to corrosion phenomena and the failure of the joints occurs by a combination of several rupture phenomena. The presence of circular cracks around the bottom of the rivet, due to the change in rivet orientation and rivet arm contact, which triggers crack initiation on this area and consequently leads to shear out failures.

Case B (primed before riveting): After exposure from 0 h to 200 h there is a negligible amount of change in mechanical property and even after 200 h of exposure the sample failed by rivet pull-out from the lower sheet. In comparison with the case A: minimum change in the clearly noticed in load–displacement curve and trace amount of corrosion product form the in overlapped sheet area.

Case C (primed after riveting): Change in load–displacement curve is negligible, however, after longer exposer (i.e. 200 h) the failure mode is very similar to case A, and salt aggregation and corrosion product observed in the overlapping area. ZM coated steel displacement also changes but negligible change occurs with the time of exposure.

It is evident from the three experiments that the material sheet primed before riveting (case B) has better corrosion resistance than the other two conditions. Between the two coatings, ZM coated steel showed better mechanical performance, which can be evident from Fig. 11. Table 4 presents the mechanical properties attained from the lap shear test, when subjected to mechanical testing. Results are omitted which fall outside the expected value. The data points that do not fall within five SD of the mean are identified as outliers. However, the results show evidence of degradation occurring due to corrosive exposure. When analysing the case B, it showed good susceptibility to corrosion resistance, which is of agreement to the visual inspection. The large standard deviation in the results, indicates that there is a differentiation in mechanical properties, when the specimens are exposed to the same conditions.

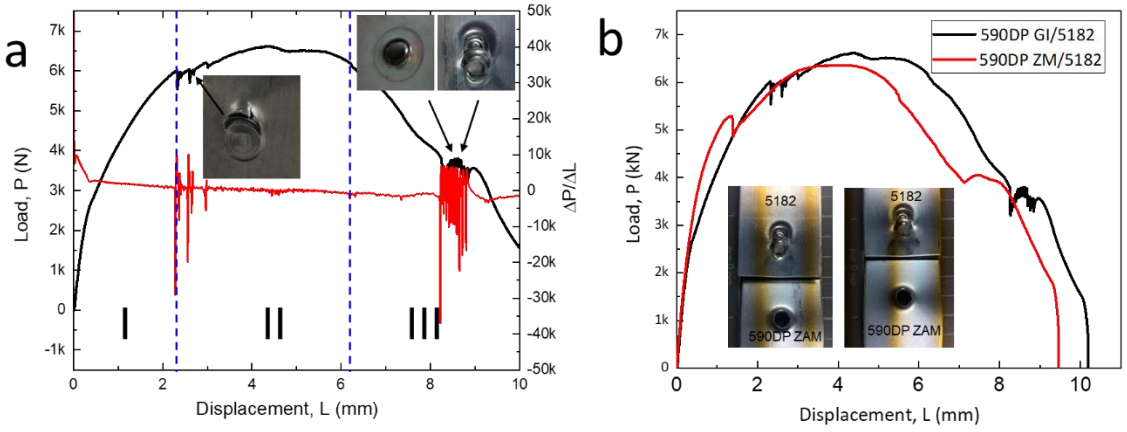

Fig. 9 Load displacement curves (a) showing various zone plots of ΔP/ΔL as a function of L illustrating actual changes at various stage of testing and (b) showing two different stakes.

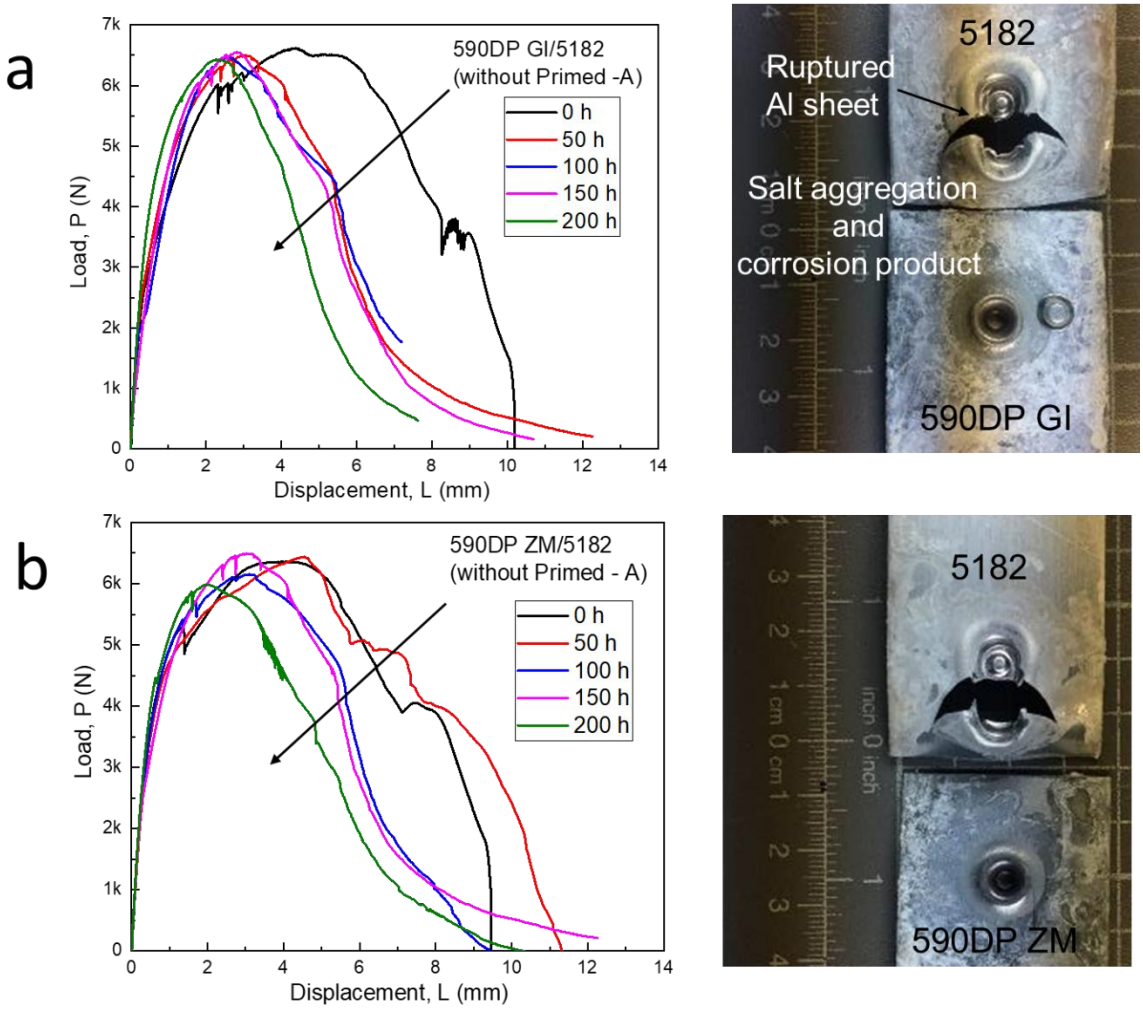

Fig. 10. Load vs displacement curves for samples without primer (case A) with increasing corrosion time (a) 590DP GI/ 5182 and (b) 590DP ZM/ 5182.

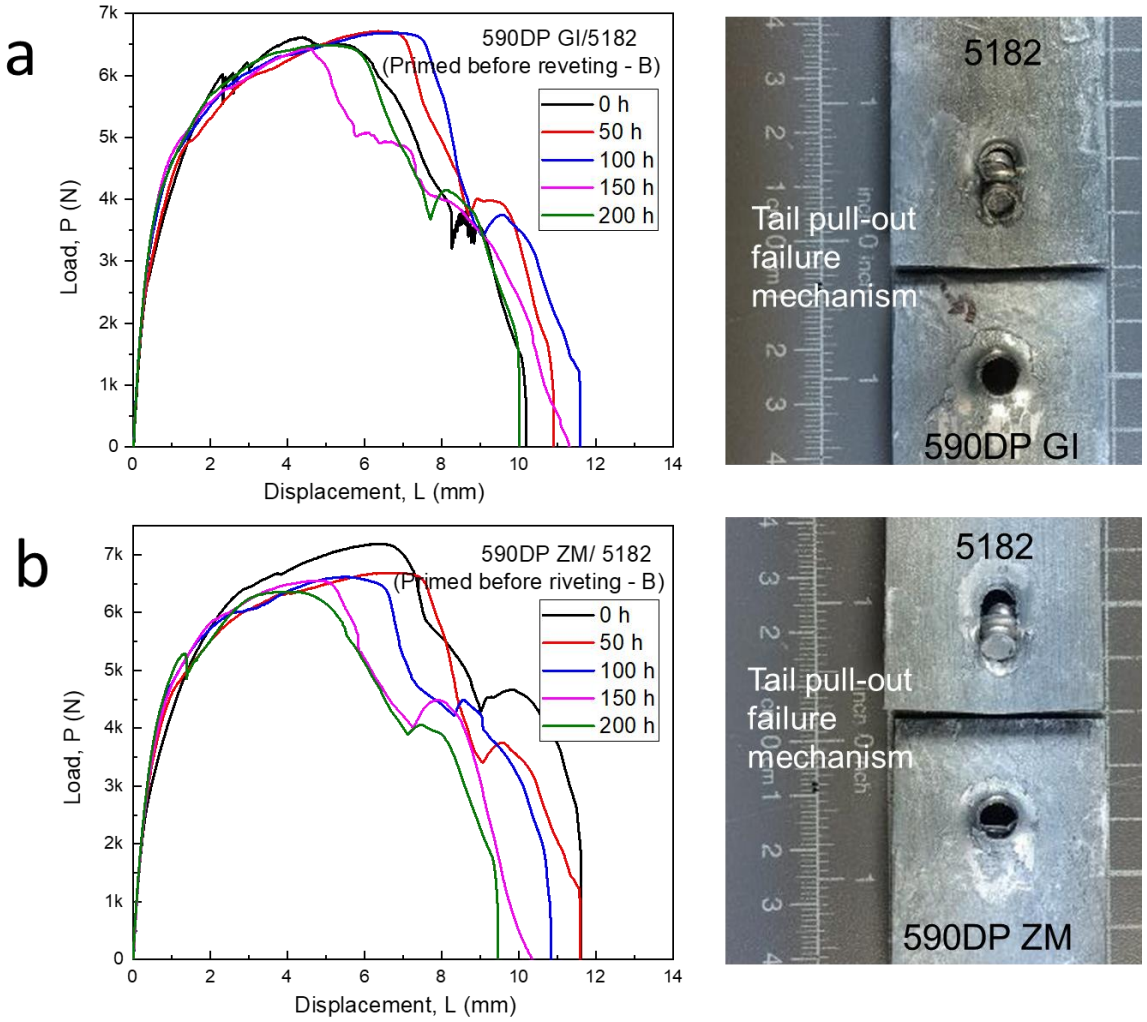

Fig. 11. Load vs displacement curves for samples with increasing corrosion time. Samples are painted with primer (both side) before riveting (case B) (a) 590DP GI/ 5182 and (b) 590DP ZM/ 5182.

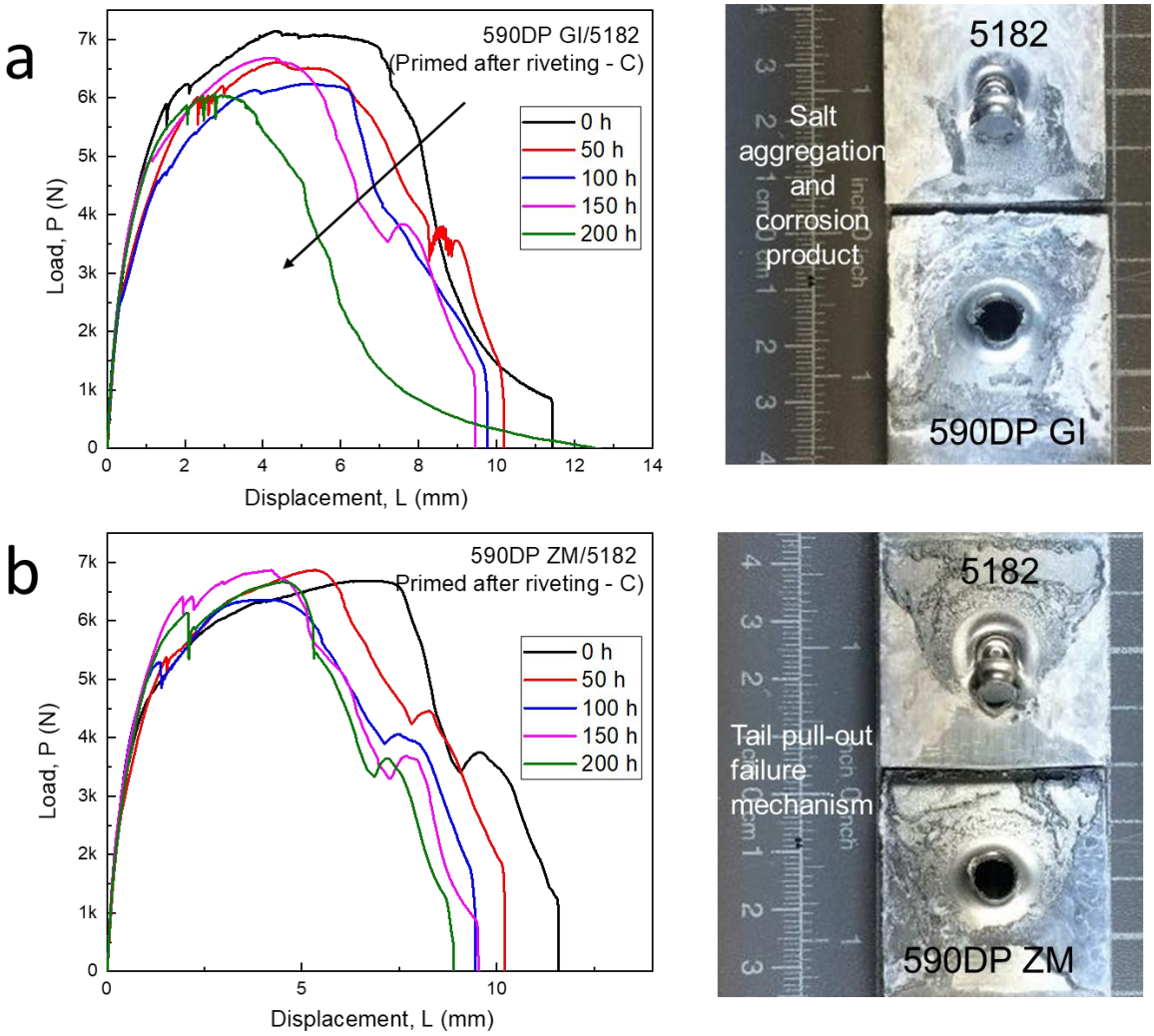

Fig. 12. Load vs displacement curves for samples with increasing corrosion time. Samples are painted with primer (both side) after riveting (case C) (a) 590DP GI/ 5182 and (b) 590DP ZM/ 5182.

Table 4. The table presents the mechanical properties acquired during the lap shear test. The ultimate tensile strength (UTS) of the joint is calculated, from the maximum initial failure. The displacement with respects to maximum load is also calculated. The standard deviation is calculated from the five tests with outliers eliminated.

		Case A		**Case B**		**Case C**	
	Exposure Time (h)	UTS (kN)	Displacement (mm)	UTS (kN)	Displacement (mm)	UTS (kN)	Displacement (mm)
GI coated	0	6.71 (± 0.2)	6.54 (± 0.6)	6.71 (± 0.2)	6.54 (± 0.6)	6.71 (± 0.2)	6.54 (± 0.6)
	50	6.51 (± 0.4)	3.03 (± 0.5)	6.61 (± 0.5)	6.34 (± 0.5)	6.61 (± 0.5)	4.4 (± 0.6)
	100	6.50 (± 0.3)	2.56 (± 0.4)	6.68 (± 0.4)	6.12 (± 0.6)	6.24 (± 0.7)	4.14 (± 0.5)
	150	6.43 (± 0.5)	2.82 (± 0.7)	6.44 (± 0.7)	5.54 (± 0.5)	6.18 (± 0.7)	4.19 (± 0.3)
	200	5.87 (± 0.7)	2.34 (± 0.4)	6.48 (± 0.8)	5.08 (± 0.7)	6.07 (± 0.6)	2.77 (± 0.5)
ZM coated	0	6.58 (± 0.2)	6.82 (± 0.4)	6.58 (± 0.2)	6.82 (± 0.4)	6.58 (± 0.2)	6.82 (± 0.4)
	50	6.44 (± 0.2)	4.54 (± 0.3)	6.39 (± 0.3)	6.46 (± 0.3)	6.38 (± 0.4)	6.64 (± 0.8)
	100	6.5 (± 0.4)	3.06 (± 0.7)	6.49 (± 0.2)	6.82(± 0.4)	6.36 (± 0.3)	5.33 (± 0.8)
	150	6.15 (± 0.4)	3.03 (± 0.7)	6.35 (± 0.2)	5.81 (± 0.8)	6.17 (± 0.4)	4.85 (± 0.4)
	200	5.98 (± 0.5)	2.32 (± 0.4)	6.46 (± 0.4)	4.86 (± 0.5)	6.27 (± 0.5)	4.54 (± 0.7)

4. Discussion

4.1 Effect of corrosion on Zn and Zn-Al-Mg coating

The results obtained for GI and ZM coated steel, corrosion formation and resistant to salt spray are significantly different and in all cases the primed samples improve resilience against degradation, and pre-riveting primed samples perform best. In order to determine the corrosion product chemical composition XRD analysis was carried out on selected samples before and after corrosion exposure. The gained X-ray diffractogram on GI and ZM samples are shown in Fig. 13 and results are summarised in Table 5. Zn coating is a reactive material and will, in absence of water, react with oxygen and form a ZnO layer on the surface. In the presence of moisture (salt spray), Zn reacts with water, to subsequently form $Zn(OH)_2$ and often the final corrosion product is $ZnCO_3$, which form $Zn(OH)_2$ reacting with CO_2 in the air [29-31].

$$Zn + 1/2O_2 + H_2O \rightarrow Zn(OH)_2 \rightarrow ZnO + H_2O \quad (2)$$

$$5ZnO + 2CO_3^{2-} + 2H^+ + 3H_2O \leftrightarrow Zn_5(CO_3)_2(OH)_6 + 2OH^- \quad (3)$$

The initial stage of corrosion forms a mixture of various corrosion products: ZnO, $Zn(OH)_2$, and hydrozincite $Zn_5(CO_3)_2(OH)_6$. In presence of salt, Na^+ (cations) and Cl^- (anions) migrate towards cathodic and Zn dissolution sites, respectively. Increasing in chloride activities and pH value of lead to form ZnO in the cathodic areas and ($Zn_5(OH)_8Cl_2 \cdot H_2O$) in the anodic area [29-32].

$$4ZnO + Zn^2 + 2Cl^- + 5H_2O \leftrightarrow Zn_5(OH)_8Cl_2 \cdot H_2O \quad (4)$$

It is evident that the phases in the ZM coating are significantly different from those in the GI coating. In ZM, the predominant phases are (see Fig. 6) Zn grains with fine Al precipitation, binary Mg_2Zn –Zn and ternary Mg_2Zn-Zn-Al eutectic and interfacial intermetallics. In the GI coating on the other hand, the predominate phases is dendritic primary Zn grain, Fig. 5. During the electrochemical reaction all phases have different properties. Experimental results (Fig. 8) shows that eutectic phase are less noble and will be anodic while Zn primary dendritic grain with Al precipitation can as sites for the catholic reactions. Under the salt contact possible reaction sequence pre-deposited NaCl, leading to dissolution of metal ions from the outermost oxide layer. This initiates electrochemical reactions on the surface, Mg is electrochemically a more active element than Zn therefore Mg dissolves first and forms magnesium hydroxide $Mg(OH)_2$ and subsequently probably transfer to $MgCO_3$ by reacting with CO_2 in the air [32-34]. However, Volvoich et. al. [33] study note that due to the limited carbonated ions concentration thus their reaction with simonkolleite

$$Zn_5(OH)_8Cl_2 \cdot H_2O + 2CO_3^{2-} + 2H^+ \leftrightarrow Zn_5(CO_3)_2(OH)_6 + 2Cl^- + 3H_2O \quad (5)$$

As a result, cathodic reaction would lead to alkaline conditions and the subsequent dissolution of Zn in form of hydrozincite. The dissolution of Mg^{2+} and Al^{3+} are expected to be responsible for the cathodic reaction and to control the pH value (avoid high value) on surface.

$$Mg^{2+} + 2OH^- \leftrightarrow Mg(OH)_2 \quad (6)$$

According to literature [33, 35, 36] the precipitation of $Mg(OH)_2$ can buffer the pH at values to those below the values necessary to transform Simonkolleite, Zinc hydroxysulfate and Hydrozincite into ZnO or $Zn(OH)_2$ at pH 7–13 in a NaCl environment. The formation of ZnO may result from the transformation of the precipitated zinc salts with advance of corrosion and an increase of pH (pH > 13):

$$Zn_5(OH)_8Cl_2 + 2OH^- \leftrightarrow 5ZnO + +2Cl^- + 5H_2O \quad (7)$$

$$Zn_5(CO_3)_2(OH)_6 + 2OH^- \leftrightarrow 5ZnO + +2HCO_3^- + 3H_2O \quad (8)$$

It is further evident from the corrosion product that after 50 h exposure the ZM sample showed an absence of ZnO compound and it was only detected after 200 h (Fig. 13b). The delay of ZnO formation is an important aspect for corrosion resistance because this transformation disturbs structure and form porosity, as shown in Fig. 8c after 100 h of salt exposure.

There is an additional possibility of simultaneous CO2 reactions with both Mg and Al to prevent a high surface pH. This is expected as the increase in the pH value in combination with the hydroxide ions within the cathodic regions can influence the stability of the formerly present chemical compounds in these regions [32, 34]. The formation of the round spots near the vicinity of the anodic sites could be attributed to the charge build up between the anode and the cathode where the metal cations flow towards the cathodic region while the hydroxide anions move towards the anode until they meet. These spots are the zinc based corrosion products. The anodic region shows the presence of cracks, holes and pits which become larger and spread over a greater surface area with the passage of time. Interestingly, the speed with which the individual patches expand seems to be related to the time at which the individual defects are formed.

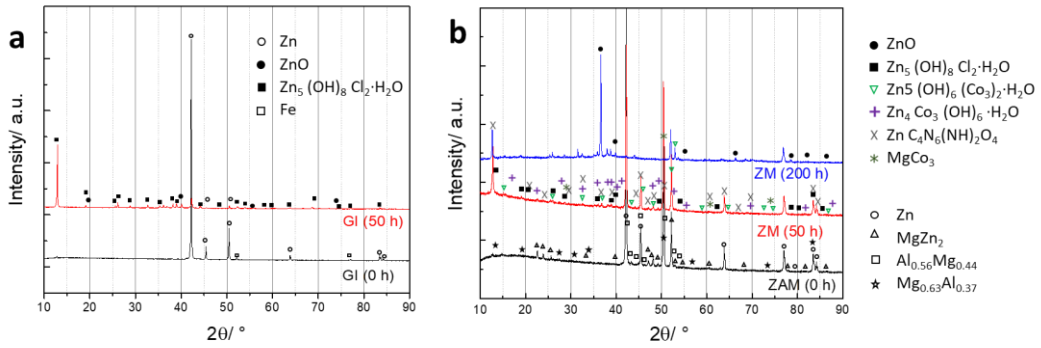

Fig. 13. X-ray diffractogram of (a) zinc (GI) and (b) zinc–aluminium–magnesium (ZM) coated steel sample surface as received and 50 and 200 h exposure to salt spray test.

Table 5. Summary of corrosion products observed by XRD on different samples. Note that some of the corrosion products are not included in figure 13 to improve the readability.

Exposure time	GI (Zn) coated	ZM (Zn-Al-Mg) coated
0 h, as received	Zn	Zn, $MgZn_2$ $Al_{0.56}Mg_{0.44}$ $Mg_{0.63}Al_{0.37}$
50 h, salt spray exposure	Zn, ZnO, $Zn_5\ (OH)_8\ Cl_2{\cdot}H_2O$, $Zn_4\ Cl\ O_4\ (OH)_7$	Zn, Al, $Zn_5\ (OH)_8\ Cl_2{\cdot}H_2O$ $Zn_5\ (OH)_6\ (Co_3)_2{\cdot}H_2O$ $Zn_4\ Co_3\ (OH)_6{\cdot}H_2O$ $Zn\ C_4N_6(NH)_2O_4$ $MgCo_3$
200 h, salt spray exposure	Zn, ZnO, $Zn_5\ (OH)_8\ Cl_2{\cdot}H_2O$, $Zn_4\ Cl\ O_4\ (OH)_7$	Zn Al, ZnO, $Zn_5\ (OH)_8\ Cl_2{\cdot}H_2O$ $Zn_5\ (OH)_6\ (Co_3)_2{\cdot}H_2O$ $Zn_4\ Co_3\ (OH)_6{\cdot}H_2O$ $Zn\ C_4N_6(NH)_2O_4$ $Zn_4Cl\ O_4\ (OH)_7$ $Zn\ (C_4\ O_4)\ (H_2O)_2$ $Zn\ (NO_3)_2\ 2HC)\ NH_2\ 2H_2O$ Zn_3P_6 $Mg\ (OH)_2$ $MgCo_3$

4.2 SPR failure mechanism and effect of corrosion

Experimentally various failure mode observed of the SPR joint under the static loading. Experimentally various failure modes were observed for the SPR joints under the static loading. During the riveting operation, sheets material go through the plastic defamation around the rivet head and tail and strength of the SPR joint primarily depend on the interlock between the bottom sheet and rivet tail. During the lap shear test both sheets were bearing against the rivet. The rivet itself was subjected to a shearing and pull-out force. This occurred due to bending and twisting, during shear testing process [37]. When the specimen underwent loading, the riveted sheets writhed under the localised yield load. The rivet was pulled out before there was adequate amount of shear force to cause the fracture of the rivet. The increase in pull-out force permitted the rivet to surpass the frictional force between the rivet shank and riveted sheets [34][23]. Thus, failure was observed as pulling out of the rivet. When analysing the rivet shank and riveted sheet, there was evidence of deformation, primarily observed at the riveted sheet. The loading force used was also consumed by friction amid the two riveted sheets [38, 39].

In the SPR joints, two possible mechanisms for corrosion the explained in literature [12]: (i) crevice corrosion due to surface irregularities or a gap between the rivet and the sheet metal and (ii) galvanic

corrosion due to use of dissimilar metal due to different electrode potentials. General conclusions can be drawn from literature is the mechanical strength is reduced, however, results varied and non-conclusive. This could be use of different alloys, different corrosion environment, exposure cycles and different method to analyse samples. Some literature provided evidence that corrosion products can tighten up the SPR joint and increase its strength [12]. This phenomenon is also evident from current experiments where corrosion product is observed around the rivet and overlap area. However, this corrosion product only helps to increase strength in initial stage and then the joints will become loose, which leads to a reduction in mechanical properties. Also observed that, in a long-term corrosive environment, exposure weakens the joints and the overlapped coating area was significantly degraded compared to the other area. In a long hours and aggressive corrosive environment likely to contribute on crack initiation through pitting and further propagation under the stress that reduced mechanical properties of the joint. Cross-section of the rivet joint is shown in Fig. 14, corrosion product around the rivet cavities are evident pitting corrosion on aluminium sheet. The aluminium matrix dissolution is induced by galvanic coupling with the Fe-rich intermetallics and steel, which favours the pitting corrosion within the matrix and an increase in oxide layer between the two sheet metals. These two phenomena lead to different kinds of fracture. Pitting corrosion/ thinning cross section area leads to crack initiation at critical areas for the joint i.e. bottom of the rivet. The thickening of the oxide layer favours unbuttoning by increasing distance of the interface. Therefore, when samples are exposed without primer (case A) they are prone to pitting and corrosion thinning which shows shear out failure and the rupture takes place at early stage. In case C, sheet material are protected with primer except overlapping area leading to a large oxide layer between the sheets and subsequently degradation of joint strength following rupturing of the aluminium sheet. In opposition, sheets primed before the SPR (case B) help to eliminate material thinning and corrosion product between the sheets, in due course SPR joints maintain original strength even after aggressive corrosion exposure. Table 6 summarised all results and associated mechanisms.

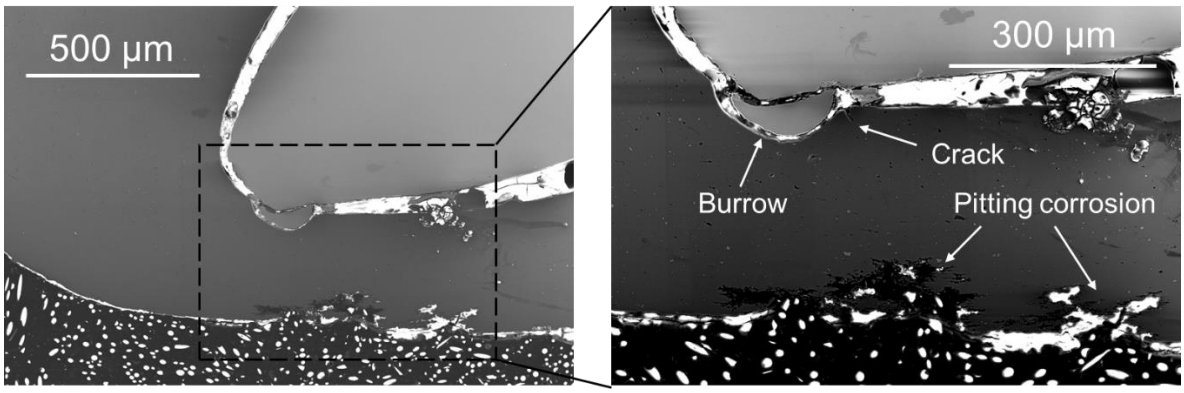

Fig. 14. Area around the bottom of the rivet 5182 aluminium sheet showing pitting corrosion, crack initiation and burrow where the rivet is in touch with the aluminium sheet. Sample was prepared after 200 h of salt spray exposure and the lap-shear test was stopped before sample failed.

Table 6. Summary of effect of corrosion environment in lap-shear test, failure and coating.

Configuration		Displacement	Failure mechanism	Corrosion product on overlapping area	Overall effect of Corrosion
As received, Case A	590DP (GI)/5182	Reduced	Al Sheet ruptured	Yes	Detrimental
	590DP (ZM)/5182	Reduced	Al Sheet ruptured	Yes	Detrimental
Painted with primer (both side) before riveting, Case B	590DP (GI)/5182	Retain	Unbuttoning	No	Good corrosion resistance
	590DP (ZM)/5182	Retain	Unbuttoning	No	Good corrosion resistance
Painted with primer after riveting (only visible area), Case C	590DP (GI)/5182	Reduced	Unbuttoning	Negligible	Partial corrosion resistance
	590DP (ZM)/5182	Reduced (negligible)	Unbuttoning	Negligible	Good corrosion resistance

5. Conclusions

The effect of accelerated corrosion on Zn and Zn-Al-Mg coating and SPR joint strength of 5182 alloy and 590DP steel were studied. Six different types of sample configurations were prepared with primer and without primers on different coated steels.

The un-primed and Zn-Al-Mg coating showed four times better corrosion resistance compared with the Zn coated steel. Distinct corrosion product were observed in both coatings. Experimental results suggests corrosion resistance Zn-Al-Mg coating enhanced due to the dissolution of eutectic to form of hydroxides on $ZnAl_2Mg_2$ and the Zn grain acted as a cathodic reduction. This process also prevented the formation of ZnO and controlled the surface pH value. Results also indicated that Zn-Al-Mg coating shows good resistance to cracks with in coating and it stops the spread of corrosion underneath the coating.

Mechanical properties of the SPR joint (the sample without primer, case A) after corrosion exposure significantly changed displacement from 10 mm to 6.5 mm. However, when the samples primed (case B) before riveting maintained original strength. Sample primed after riveting (case C) also reduced properties but less compared to case A and specifically Zn-Al-Mg coated sample which show minimum reduction on displacement. Sheet material primed before the riveting showed remarkable resistance to corrosion in comparison with A and C. The corrosion resistance trends are B > C > A; ZM > GI.

Results provided evident from 5182 sheet (lower sheet) that pitting corrosion on surface play important role in mechanical property. Anodic reactivity on the 5182 aluminium alloy surface increases due to the presence of $Al_6(Fe,Mn)$ intermetallics particles and these particles act as pit initiation sites and under the load they are likely to form cracks from there.

Acknowledgement

The key funding of this project as well as the supply of the materials is from POSCO steel South Korea. In addition to that, the characterisation and joining instrumental facility is supported from the Higher Education Funding Council for England (HEFCE) fund and the WMG Centre High Value Manufacturing Catapult is gratefully acknowledged.

References

[1] S.A. Shaheen, T.E. Lipman, Reducing greenhouse emissions and fuel consumption: Sustainable approaches for surface transportation, IATSS Research 31(1) (2007) 6-20.
[2] European Commission Climate Action—Paris Agreement, 2015.
[3] T. Sakurai, The latest trends in aluminium alloy sheets for automotive body panels, Kobelco Technology Review 28 (2008) 22-28.
[4] J. Davis, ASM Specialty Handbook: Aluminum and Aluminum Alloys, ASM International (1993).
[5] H.K.D.H. Bhadeshia, Problems in the Welding of Automotive Alloys, Science and Technology of Welding and Joining 20(6) (2015) 451-453.
[6] EAA Aluminium Automotive Manual – Joining dissimilar materials, The Aluminium Automotive Manual 2015.
[7] N.T. Williams, J.D. Parker, Review of resistance spot welding of steel sheets Part 1 Modelling and control of weld nugget formation, International Materials Reviews 49(2) (2004) 45-75.
[8] C. Bagger, F.O. Olsen, Review of laser hybrid welding, Journal of Laser Applications 17(1) (2005) 2-14.
[9] J. Mazumder, Laser Welding: State of the Art Review, JOM 34(7) (1982) 16-24.
[10] E. Karadeniz, U. Ozsarac, C. Yildiz, The effect of process parameters on penetration in gas metal arc welding processes, Materials & Design 28(2) (2007) 649-656.
[11] P.L. Threadgill, A.J. Leonard, H.R. Shercliff, P.J. Withers, Friction stir welding of aluminium alloys, International Materials Reviews 54(2) (2009) 49-93.
[12] D. Li, A. Chrysanthou, I. Patel, G. Williams, Self-piercing riveting-a review, The International Journal of Advanced Manufacturing Technology 92(5) (2017) 1777-1824.
[13] I. Papadimitriou, P. Efthymiadis, H.R. Kotadia, I.R. Sohn, S. Sridhar, Joining TWIP to TWIP and TWIP to aluminium: A comparative study between joining processes, joint properties and mechanical performance, Journal of Manufacturing Processes 30 (2017) 195-207.
[14] E.C. Ozkat, P. Franciosa, D. Ceglarek, Laser dimpling process parameters selection and optimization using surrogate-driven process capability space, Optics & Laser Technology 93 (2017) 149-164.
[15] H. Zhao, D.R. White, T. DebRoy, Current issues and problems in laser welding of automotive aluminium alloys, International Materials Reviews 44(6) (1999) 238-266.
[16] S.D. Meshram, T. Mohandas, G.M. Reddy, Friction welding of dissimilar pure metals, Journal of Materials Processing Technology 184(1) (2007) 330-337.
[17] R.S. Mishra, Z.Y. Ma, Friction stir welding and processing, Materials Science and Engineering: R: Reports 50(1) (2005) 1-78.
[18] L. Han, M. Thornton, M. Shergold, A comparison of the mechanical behaviour of self-piercing riveted and resistance spot welded aluminium sheets for the automotive industry, Materials & Design 31(3) (2010) 1457-1467.
[19] L. Krüger, M. Mandel, Electrochemical behaviour of aluminium/steel rivet joints, Corrosion Science 53(2) (2011) 624-629.
[20] L. Calabrese, E. Proverbio, G. Di Bella, G. Galtieri, C. Borsellino, Failure behaviour of SPR joints after salt spray test, Engineering Structures 82 (2015) 33-43.
[21] T. Prosek, D. Persson, J. Stoulil, D. Thierry, Composition of corrosion products formed on Zn–Mg, Zn–Al and Zn–Al–Mg coatings in model atmospheric conditions, Corrosion Science 86 (2014) 231-238.

[22] L. Calabrese, L. Bonaccorsi, E. Proverbio, G. Di Bella, C. Borsellino, Durability on alternate immersion test of self-piercing riveting aluminium joint, Materials & Design 46 (2013) 849-856.
[23] E.V. Stephens, 2 - Mechanical strength of self-piercing riveting (SPR), in: A. Chrysanthou, X. Sun (Eds.), Self-Piercing Riveting, Woodhead Publishing2014, pp. 11-32.
[24] M. Mandel, L. Krüger, Long-term Corrosion Studies of a CFRP/EN AW-6060-T6 Self-piercing rivet Joint and a Steel/EN AW-6060-T6 Blind Rivet Joint, Materials Today: Proceedings 2 (2015) S131-S140.
[25] ASTM B117 - 16: Standard Practice for Operating Salt Spray (Fog) Apparatus.
[26] EN ISO 12273:2001. Specimen dimensions and procedure for shear testing resistance spot, seam and embossed projection welds.
[27] S.M.A. Shibli, B.N. Meena, R. Remya, A review on recent approaches in the field of hot dip zinc galvanizing process, Surface and Coatings Technology 262 (2015) 210-215.
[28] G.L. Kulak, J.W. Fisher, J.H.A. Struik, Guide to design criteria for bolted and rivetd joints, New York, Wiley, Inc. (1987).
[29] I. Odnevall, C. Leygraf, Formation of NaZn4Cl(OH)6SO4 · 6H2O in a marine atmosphere, Corrosion Science 34(8) (1993) 1213-1229.
[30] T.E. Graedel, Corrosion Mechanisms for Zinc Exposed to the Atmosphere, Journal of The Electrochemical Society 136(4) (1989) 193C-203C.
[31] J.E. Svensson, L.G. Johansson, A laboratory study of the initial stages of the atmospheric corrosion of zinc in the presence of NaCl; Influence of SO2 and NO2, Corrosion Science 34(5) (1993) 721-740.
[32] E. Diler, B. Rouvellou, S. Rioual, B. Lescop, G. Nguyen Vien, D. Thierry, Characterization of corrosion products of Zn and Zn–Mg–Al coated steel in a marine atmosphere, Corrosion Science 87 (2014) 111-117.
[33] P. Volovitch, T.N. Vu, C. Allély, A. Abdel Aal, K. Ogle, Understanding corrosion via corrosion product characterization: II. Role of alloying elements in improving the corrosion resistance of Zn–Al–Mg coatings on steel, Corrosion Science 53(8) (2011) 2437-2445.
[34] S. Schuerz, M. Fleischanderl, G.H. Luckeneder, K. Preis, T. Haunschmied, G. Mori, A.C. Kneissl, Corrosion behaviour of Zn–Al–Mg coated steel sheet in sodium chloride-containing environment, Corrosion Science 51(10) (2009) 2355-2363.
[35] M. Salgueiro Azevedo, C. Allély, K. Ogle, P. Volovitch, Corrosion mechanisms of Zn(Mg, Al) coated steel in accelerated tests and natural exposure: 1. The role of electrolyte composition in the nature of corrosion products and relative corrosion rate, Corrosion Science 90 (2015) 472-481.
[36] M. Salgueiro Azevedo, C. Allély, K. Ogle, P. Volovitch, Corrosion mechanisms of Zn(Mg,Al) coated steel: 2. The effect of Mg and Al alloying on the formation and properties of corrosion products in different electrolytes, Corrosion Science 90 (2015) 482-490.
[37] R. Porcaro, A.G. Hanssen, M. Langseth, A. Aalberg, An experimental investigation on the behaviour of self-piercing riveted connections in aluminium alloy AA6060, International Journal of Crashworthiness 11(5) (2006) 397-417.
[38] D. Li, L. Han, M. Thornton, M. Shergold, G. Williams, The influence of fatigue on the stiffness and remaining static strength of self-piercing riveted aluminium joints, Materials & Design (1980-2015) 54 (2014) 301-314.
[39] D. Li, Influence of local surface texture by tool impression on the self-piercing riveting process and the static lap shear strength, Journal of Manufacturing Processes 29 (2017) 298-309.